JOURNAL OF OPTOELECTRONICS AND ADVANCED MATERIALS Vol. 12, No. 12, December 2010, p. 2456 - 2461

Numerical simulation of a DFB-fiber laser sensor (II) – theoretical analysis of an acoustic sensor

I. LANCRANJAN[*], S. MICLOS[a], D. SAVASTRU[a], A. POPESCU[a]
Advanced Study Center–National Institute of Aerospace Research "Elie Carafoli",
220 Iuliu Maniu Boulevard, Bucharest, Romania
[a] *National Institute R&D of Optoelectronics, INOE 2000, 409 Atomistilor str.,*
P. O. Box MG. 5, Magurele-Ilfov, Romania

This paper is the second of a series on numerical simulation of distributed feedback fiber laser (DFB-FL) sensors and their applications, especially in aeronautics. Here the developed numerical analysis of a DFB-FL air acoustic sensor is presented. The main purpose of the performed theoretical analysis consists into a better understanding of DFB-FL itself and of its interaction with environment in order to be operated as an air acoustic sensor.

(Received November 22, 2010; accepted November 30, 2010)

Keywords: DFB-FL, numerical simulation, laser acoustic sensor, aeronautical application

1. Introduction

This paper is the second one of a series pointing to reach an improved design of fiber optic sensors [1] used for various applications, in this case acoustic sensors. This paper contains preliminary results obtained in numerical simulation of Distributed FeedBack Fiber Lasers (DFB-FL) used as acoustic sensors. Since the earliest papers on fiber-optic acoustic sensors more than 20 years ago [2], most of the attention in the field has been on interferometric hydrophones [3-5]. These devices have high sensitivities, but they require sensor heads in which the smallest dimension is typically large compared with the fiber diameter and rather complex readout systems. In contrast to interferometric sensors, fiber Bragg grating sensors [6, 7] can easily be used for quasi distributed sensing by means of writing many gratings along a single fiber. However, although some research has been done on the sensing of high acoustic pressures [8, 9] and on sensors in which the variation of the reflected intensity is measured [10], the bandwidth of Bragg grating reflection spectra is generally too large to yield a satisfactory resolution for acoustic sensing without the use of sensitivity-enhancing sensor heads [11]. The line width of a DFB-FL can be considerably narrower than the bandwidth of the reflected signals from passive Bragg gratings, and fiber Bragg grating lasers are therefore possibly an attractive alternative for acoustic sensing. As is the case of other fiber Bragg grating devices, the sensors can easily be multiplexed and used for quasistatic sensing [12–14]. There are, however, still some unresolved questions regarding the stability of remotely pumped systems [15].

Fiber DFB lasers have the advantage of stable lasing in a single longitudinal mode and, in addition, have a relatively short sensitive cavity length. The latter is important when measuring high-frequency acoustic fields. The response of the fiber lasers' frequencies to acoustic signals in air was numerically simulated. Because of the rather high compressibility of air, thermally induced frequency shifts of the lasers have to be taken into account in addition to the pressure-induced shifts.

A potential application of this kind of devices could be acoustic sensing in aeronautics and hostile industrial environments. It is also important to understand the response when acoustic fields represent a noise source. Such acoustic noise can enhance the frequency noise of DFB-FL used as sources, but with proper packaging this acoustically induced frequency noise can be reduced. The investigated DFB-FL air acoustic sensor configuration was uncoated, but the presented theoretical analysis can easily be extended to fibers with coatings.

The interaction of acoustic air pressure wave with the optic fiber is theoretically analyzed. The main idea of the presented theoretical analysis is that the interaction between the DFB-FL acoustic sensor and the environment (depending on the distance from the DFB-FL acoustic sensor) can be considered as adiabatic. The necessary conditions where this hypothesis is correct are presented.

2. Theory

In Fig. 1 the schematic of the considered DFB-FL acoustic sensor is presented. It is necessary to point out that in the DFB-FL acoustic sensor placed into a certain air environment, two zones have to be considered: one in the near proximity of the optic fiber and the second one far away of it. It can be considered without loss of generality that when the pressure of the air varies due to the acoustic wave the work done to compress and decompress the air leads to temporal temperature variations of the DFB-FL environment [16]. These temperature variations follow the first principle of thermodynamics, which is expressed as [17]

$$dq = \rho c_V dT + (c_P - c_V)\rho\left(\frac{\partial T}{\partial V}\right)_P dV \\ = \rho c_P dT - (c_P - c_V)\rho \frac{T}{p} dp \tag{1}$$

In Eq.(1) dq is the heat added per unit volume, T is the temperature, p is the pressure, ρ is the density of mass, c_P and c_V are the specific-heat capacities at constant pressure and volume, respectively. In the last line of Eq. (1) the ideal-gas-law approximation of constant pV/T is used.

The term dq must equal the heat transferred from the surroundings [18]:

$$dq = (\kappa \nabla^2 T)dt + dq_{conv} \tag{2}$$

In Eq. (2) κ is the thermal conductivity and dq_{conv} is the heat transfer resulting from convection. Because of the time scale of the acoustic pressure wave, the latter term is ignored here. Explicitly, the convection is a much slower process in comparison with acoustic wave pressure variations. For low acoustic pressures compared with the static pressure, which is the most usual situation, we can set the value of T/p as

$$\frac{T}{p} = \frac{T_{static}}{p_{static}} \tag{3}$$

By splitting the temperature and the pressure into static components (T_{static} and p_{static}, respectively), considering the harmonically variation of the acoustic components ($\Delta T(r)e^{(i\omega t)}$ and $\Delta p(r)e^{(i\omega t)}$, respectively) and combining Eqs. (1) and (3), we get [16]

$$T(r,t) = T_{static} + \Delta T(r)e^{(i\omega t)} \tag{4}$$

$$p(r,t) = p_{static} + \Delta p(r)e^{(i\omega t)} \tag{5}$$

$$(i\omega \Delta T) = D_{T_{air}} \nabla^2(\Delta T) + (i\omega \Delta T_0) \tag{6}$$

$$D_{T_{air}} = \frac{\kappa}{\rho \cdot c_P} \tag{7}$$

$$\Delta T_0 = \frac{c_P - c_V}{c_P} \frac{T_{static}}{p_{static}} \Delta p \tag{8}$$

In Eqs. (4) – (8) $D_{T_{air}}$ is the thermal diffusivity of air and typically has a value of $22.5\times10^{-6} m^2 s^{-1}$ at 300 K [18]. In Eq. (6) ω is the acoustic angular frequency. Far away from the fiber, we can neglect the Laplacian term $\nabla^2(\Delta T)$ in Eq. (6) and thus assume that the process is adiabatic if

$$\frac{D_{T_{air}}\left(\frac{\omega}{c_{sound}}\right)^2}{\omega} = \frac{D_{T_{air}}(2\pi f)}{c_{sound}^2} = \frac{\left(22.5\times10^{-6} m^2/s\right)2\pi f}{\left(350\, m/s\right)^2} = \frac{f}{0.87\text{GHz}} << 1 \tag{9}$$

In expression (9), c is the velocity of sound, and typical values [18] for air at 300 K have been inserted. From Eq. (9), we can see that the adiabatic assumption implies that $\Delta T \approx \Delta T_0$. It is then trivial to calculate the Laplacian because ΔT_0 is proportional to the acoustic pressure and harmonic. Thus, for frequencies up to several megahertz, the only significant contribution to the Laplacian term in Eq.(9) comes from the fact that the medium becomes inhomogeneous because of the presence of optical fiber.

In this paper we study acoustic frequencies in the range of 100 Hz to 20 kHz. Thus the acoustic wavelength is large compared with the fiber diameter, and we can ignore the spatial dependence of the acoustic pressure in the vicinity of the fiber. The temperature field is spatially dependent on only the radial distance r from the fiber axis, and Eq. (9) reduces its form to an inhomogeneous Bessel equation of the zeroth order with the general solution

$$\Delta T_{air}(r) = \Delta T_0 + C_1 J_0\left[\left(\sqrt{\frac{\omega}{iD_{T_{air}}}}\right)r\right] + C_2 Y_0\left[\left(\sqrt{\frac{\omega}{iD_{T_{air}}}}\right)r\right] \tag{10}$$

In silica there is no significant acoustical generation of heat, and thus the temperature in the fiber is determined from a homogeneous Bessel equation with the general solution

$$\Delta T_{fiber}(r) = C_3\left\{J_0\left[\left(\sqrt{\frac{\omega}{iD_{T_{air}}}}\right)r\right]\right\} + C_4\left\{Y_0\left[\left(\sqrt{\frac{\omega}{iD_{T_{air}}}}\right)r\right]\right\} \tag{11}$$

The expression $D_{T_{silica}} = 0.834\times10^{-6} m^2/s$ [18] is the thermal diffusivity of fused silica. The constants $C_{1,2,3,4}$ in Equations (10.1.11) and (10.1.12) are found by use of the boundary condition $\lim_{r\to\infty} \Delta T(r) = \Delta T_0$ and by the requirement that both $T(r)$ and its derivative are finite and continuous everywhere. This condition yields

$$C_1 = \frac{T_0}{\left(\frac{J_0(\zeta_{silica})H_1^{(2)}(\zeta_{air})}{J_1(\zeta_{silica})}\right)\sqrt{\frac{D_{T_{silica}}}{D_{T_{air}}}} - H_0^{(2)}(\zeta_{air})} \tag{12}$$

$$C_2 = -iC_1 \tag{13}$$

$$C_3 = \frac{T_0}{J_0(\zeta_{silica}) - \left(\frac{J_1(\zeta_{silica})H_0^{(2)}(\zeta_{air})}{H_1^{(2)}(\zeta_{air})}\right)\sqrt{\frac{D_{T_{air}}}{D_{T_{silica}}}}} \tag{14}$$

$$C_4 = 0 \tag{15}$$

$$\zeta_{air} = R\sqrt{\frac{\omega}{iD_{T_{air}}}} \tag{16}$$

$$\zeta_{silica} = R\sqrt{\frac{\omega}{iD_{T_{silica}}}} \tag{17}$$

where R is the fiber radius, which in our case is $62.5\mu m$ and $H_i^{(2)}$ is the second Hankel function of the order i.

The total frequency shift of the laser at the acoustic frequency can be found by the addition of the frequency shifts caused by the temperature and the pressure variations in the fiber. The dc temperature sensitivity of the laser frequency ν of a fiber laser at constant pressure p and longitudinal stress σ_{zz} is

$$\left(\frac{\Delta\nu}{\nu}\right)_{\sigma_{zz},p} = -\left[\frac{\partial \in_{zz}}{\partial T} + \frac{1}{n_{eff}}\left(\frac{\partial n_{eff}}{\partial T}\right)_{\sigma_{zz},p}\right]\Delta T = -(\alpha+\xi)\Delta T \qquad (18)$$

where $\in_{zz}$ is the temperature-shift-induced strain along the longitudinal axis (which also equals the strain along the other axes), $n_{eff} \approx 1.465$ is the effective modal refractive index, α is the thermal-expansion coefficient (typically equal to $0.55\times10^{-6}K^{-1}$ for silica [19-25]), and ξ is the thermo-optic coefficient. The subscripts σ_{zz} and p indicate constant longitudinal stress and pressure, respectively. If the fiber is axially constrained, i.e., $\in_{zz}$ is constant, the dc temperature sensitivity equals

$$\left(\frac{\Delta\nu}{\nu}\right)_{\in_{zz},p} = -(p_e+\xi)\Delta T \qquad (19)$$

$$p_e = \frac{n^2}{2}\left[p_{12} - \mu(p_{11}+p_{12})\right] \approx 0.22 \qquad (20)$$

where $p_{11} \approx 0.27$ and $p_{12} \approx 0.12$ [26] are the diagonal and the off-diagonal elements, respectively, of the elastic-optical tensor of silica and $\mu = 0.17$ is the Poisson ratio. Note that, although $\in_{zz}$ is constant, the strain in other directions may vary.

In our harmonically varying heat-diffusion case the temperature is not spatially uniform over the fiber cross section. This non-uniformity leads to stress and strain even in parts of the fiber cross section where the temperature fluctuations are small. The laser frequency shift in this case equals

$$\left(\frac{\Delta\nu}{\nu}\right)_{\in_{zz},p} = -\left[\xi + (p_{11}+2p_{12})\frac{n^2}{2}\alpha\right]\Delta T - \left(1 - p_{12}\frac{n^2}{2}\right)\in_{zz} + (p_{11}+2p_{12})\frac{n^2}{2}\in_{rr} \qquad (21)$$

where $\in_{zz}$ is the temperature-induced strain along a transverse axis, $\in_{zz} = 0$ in the axially constrained case.

It is difficult to make exact predictions of this thermally induced strain in a fiber with multiple dopants. In particular, the thermal-expansion coefficient is expected to be non-uniform over the cross section of the fiber. For simplicity, we used the expansion coefficient and the elastic constants of silica, including a Young's modulus of 72 GPa, throughout the fiber. The strain was calculated by division of the fiber radius r into 5000 sections and the assumption of constant temperature within each section. In each layer i the strain is then given by the Lame´ solution [27, 28]:

$$\in_{rr;j} = K_{1;j} + \frac{K_{2;j}}{r^2} \qquad (22)$$

$$\in_{\theta\theta;j} = K_{1;j} - \frac{K_{2;j}}{r^2} \qquad (23)$$

$$\in_{zz;j} = K_{3;j} \qquad (24)$$

where $K_{1;j}$, $K_{2;j}$ and $K_{3;j}$ are constants and $\in_{rr;j}$, $\in_{\theta\theta;j}$ and $\in_{zz;j}$ are the radial, the azimuthally, and the longitudinal strains, respectively, in the fiber. Clearly $\in_{zz;j}$ and thus $K_{3;j}$ must be constant in a transverse cross section of the fiber, and $K_{2;j}$ has to be zero in the innermost layer. In addition, the radial stress and the azimuthally strain have to be continuous. By applying these boundary conditions, we can find the strain and thus the total temperature-induced frequency shift.

The frequency shift resulting from the thermally induced strain is shown in Figures 3 and 4 for the axially free and the constrained cases, respectively. The considered universal numerical constants, with $\xi = 5.1\times10^{-6}K^{-1}$, were used in the calculations. In the same figures the strain-independent term of Eq. 21) is plotted. As can be seen from the figures, the strain in the core decreases more slowly than does the temperature.

The reason is that the strain is dependent on the temperature throughout the whole fiber cross section, including the core containing the Bragg grating and the clad. At higher frequencies the thermally induced strain is therefore more important than the temperature fluctuations in the core. At approximately 1 kHz the temperature at the surface of the fiber and in the core is π out of phase for the first time, which causes a dip in the radial-strain curves.

If we use only the values of strain and temperature in the center of the fiber in Eq. (21), we introduce errors because the optical mode has a finite confinement. The errors can be corrected by the assumption of a Gaussian optical mode [29] and by integration over the fiber cross section of the product of the mode intensity and the frequency shift given by Eq. (21). This correction was, however, found to be negligible.

To find the total frequency shift, we also have to add the contribution from the acoustic pressure. Because the wavelength of the acoustic wave is much larger than the diameter of the fiber, we assume that the pressure is uniform over the fiber cross section. For an axially constrained fiber, the pressure sensitivity has a predicted value of $(\Delta\nu/\nu)_{e,T} = -4.5\times10^{-12}$ Pa^{-1}, whereas the predicted value for an axially free fiber is $(\Delta\nu/\nu)_{p,T} = 2.7\times10^{-12}$ Pa^{-1} In Figs. 4 and 5 the total and the pressure dependent frequency shifts for the axially free and the constrained cases, respectively, are plotted. As can be seen from the figures, thermal effects dominate over direct pressure for all measured frequencies for a fiber free to expand, but the thermal effects have less importance for acoustic frequencies higher than 3 kHz for the axially constrained case. The reason for the difference is the thermally induced longitudinal strain for the fiber that is free to expand.

3. Numerical simulation results.

Numerical simulations were performed for optical fiber doped with erbium ions (Er^{3+}). The considered DFB-FL acoustic sensor has an overall diameter of 125 μm, with a core of 8 μm diameter. The Bragg grating spatial modulation wavelength (Λ) was considered as 500 nm. The numerical simulations were performed using 1.550 μm as the laser operating wavelength.

The numerical simulations were performed using the SCILAB and MATLAB software packages.

In Fig. 1 the schematic of the investigated acoustic DFB-FL sensor is presented.

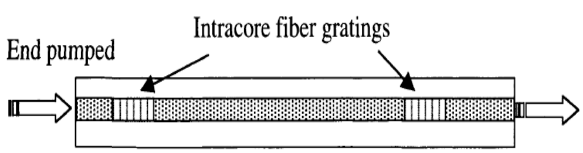

Fig. 1. Schematic representation of the investigated acoustic DFB-FL sensor.

In Fig. 2 the temperature transfer functions at $T = 300K$ are plotted against the *r* for acoustic frequencies of *f*=100 Hz and *f*=20 kHz. The parameters listed in Table 1 were used in the calculations. The amplitude of the transfer function at the center of the fiber is plotted versus the frequency in Fig. 2. From the figures we can clearly see that the diffusion of heat to the core is an effect that is a low pass filter in frequency. This fact is a consequence of the slowness of heat diffusion in comparison with the considered acoustic pressure wave characteristic times [16].

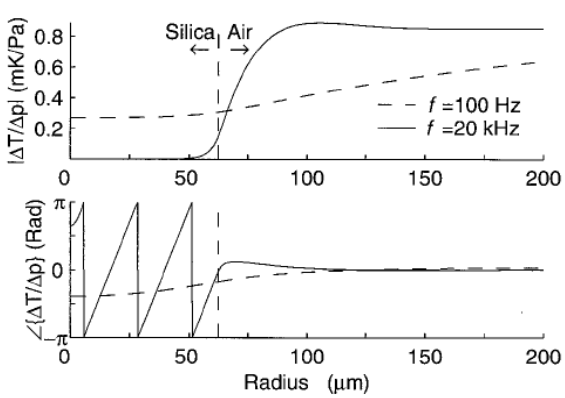

Fig. 2. $\Delta T/\Delta p$ as a function of the radius r at acoustic frequencies of 100 Hz and 20 kHz for a stripped fiber with a radius of 62.5 μm and embedded in air at T = 300 K.

As can be easily observed in Fig. 2, the phase of the transfer function exhibits small spatial variation across the fiber for lower frequencies, but for *f*=20 kHz the spatial phase variation is more rapid.

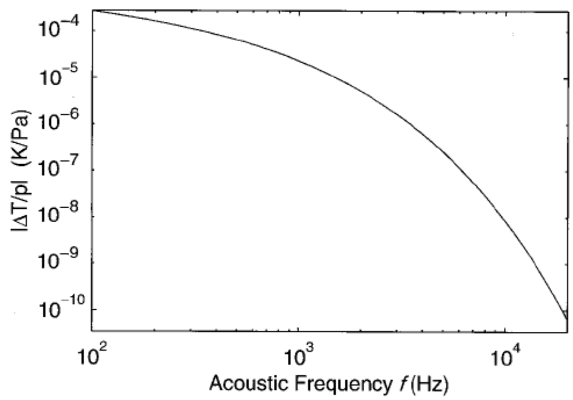

Fig. 3. $\Delta T/\Delta p$ variation for the same DFB-FL configuration fiber as that of Fig. 2.

In Figs. 3, 4 and 5 are presented numerically simulated parameters of the studied DFB-FL structure as functions of acoustic frequency. In Fig. 3 the relative variation of temperature versus acoustic wave pressure variation. In Fig. 4 the relative frequency laser shift is presented as a function of considered acoustic frequency. In Figs. 4 and 5 the frequency laser shift variations versus the acoustic frequency are presented for the cases of the optic fiber with and without constrain.

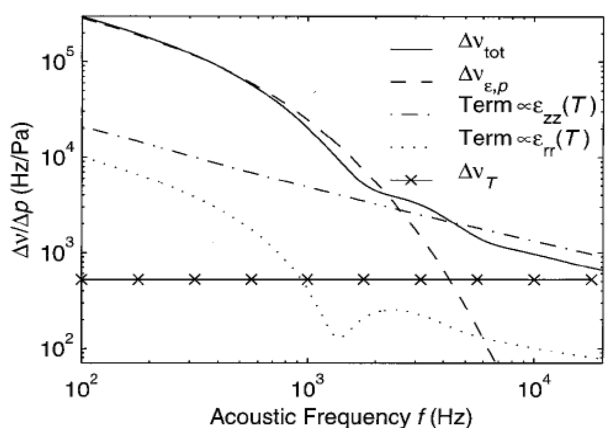

Fig. 4. Contributions to the total frequency shift $\Delta\nu_{tot}/\Delta p$ of a fiber laser made of the same fiber as that of Fig. 1 and embedded in air with acoustic waves. The contributions from the acoustic pressure $\Delta\nu_T$ and the three thermally induced terms of Eq.(11), which are the strain-independent term $\Delta\nu_{e,p}$ and the terms proportional to ϵ_{rr} and ϵ_{zz} are plotted. The fiber is axially free.

The influence of the exposure of the DFB-FL sensor structure to an acoustic wave is illustrated in Figs. 6 and 7.

The RMS frequency shift strongly decreases with acoustic frequency.

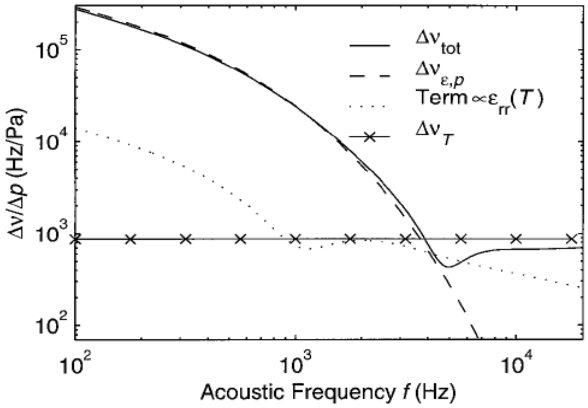

Fig. 5. Same as for Fig. 4 but with the fiber axially constrained.

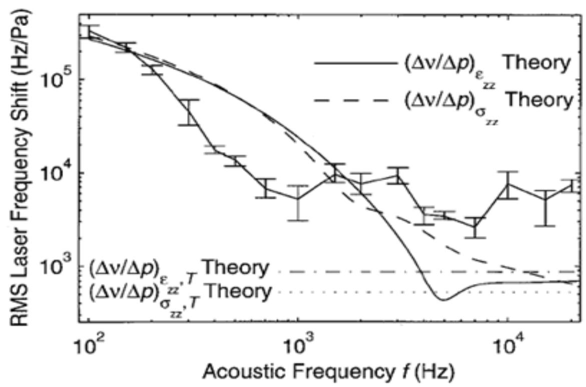

Fig. 6. Theoretical frequency shifts of DFB-FL sensor structure when exposed to an acoustic wave. The error bars show the extreme estimated data.

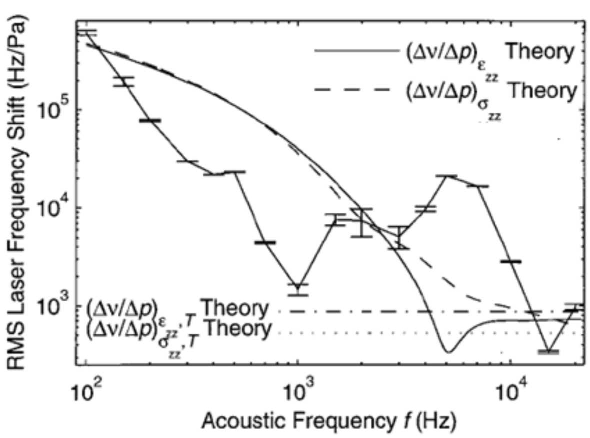

Fig. 7. Same as for Fig. 6 but for a modified DFB-FL structure.

Figure 8 presents the NEP and the frequency noise determined by the acoustic wave. As it can be observed in this figure, the NEP is stabilized and the frequency noise is relatively small because the amplitude of the oscillations of the acoustic wave generated by pressure and temperature are small compared to the pressure and temperature of the environment (p and T static).

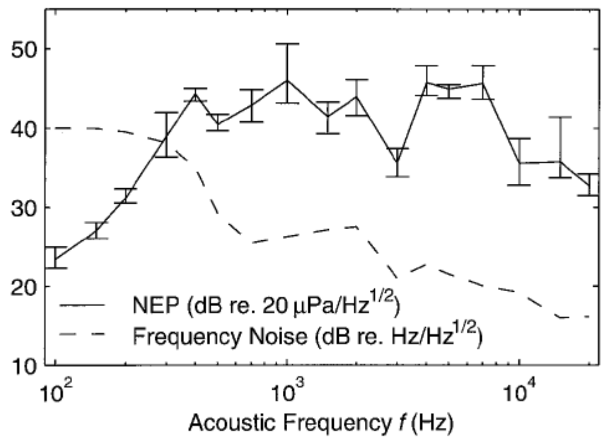

Fig. 8. NEP determined by use of the acoustic sensitivity and typical noise spectrum for studied fiber DFB-FL structure.

Temperature gradient in air at the fiber surface that are due to pure diffusion and to free and forced convection is presented in Fig. 9 versus the acoustic pressure and in Fig. 10 versus the acoustic frequency. The linearity observed in Fig. 9 is due to the fact that the phenomenon is quasi adiabatic.

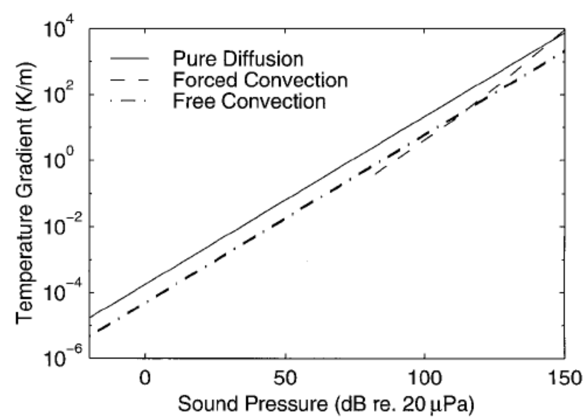

Fig. 9. Temperature gradients in air at the fiber surface that are due to pure diffusion and to free and forced convection with f = 100 Hz versus the acoustic pressure. The gradients are calculated by use of the theory of Section 2. The free convection is calculated for dc temperature differences of 1, 5, and 10 K between the fiber surface and air, but the three curves overlap.

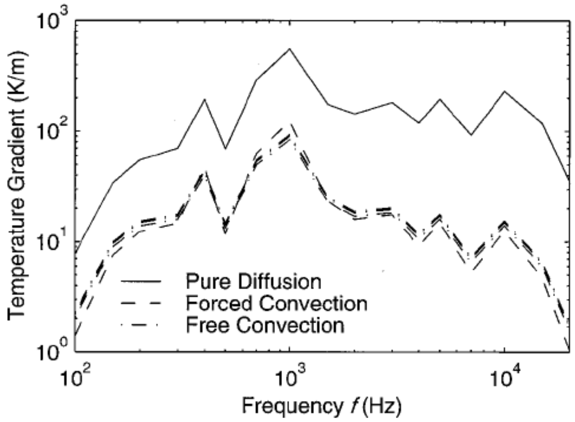

Fig. 10. Same temperature gradients as for Fig. 9 at different acoustic pressures versus the acoustic frequency. The pressure was considered in the range 85–125 dB re. 20 μPa.

One important observation to be underlined is that a series of parameters describing the function of DFB-FL as an acoustic sensor can be simulated, but a certain limitation is imposed by the possible experimental setup in the sense that some of them are difficult to be measured.

4. Conclusions

The presented results concerning the numerical simulation of DFB-FL acoustic sensor structure will be further developed by designing an experimental device dedicated to aeronautical applications.

References

[1] I. Lancranjan, S. Miclos, D. Savastru, J. Optoelectron. Adv. Mater., **12**(8), 1636 (2010.
[2] J. A. Bucaro, H. D. Dardy, and E. F. Carome, J. Acoust. Soc. Am. **62**, 1302 (1977).
[3] A. D. Kersey, Opt. Fiber Technol**. 2**, 291 (1996).
[4] S. Knudsen, K. Bløtekjær, J. Lightwave Technol. **12**, 1696 (1994).
[5] S.-T. Shih, Opt. Eng. **37**, 968 (1998).
[6] W. W. Morey, G. Meltz, and W. H. Glenn, Fiber Optic and Laser Sensors VII, R. P. DePaula, E. Udd, eds., Proc. SPIE 1169, 98–107, 1989.
[7] A. D. Kersey, M. A. Davis, H. J. Patrick, M. L. K. P. Koo, C. G.Askins, M. A. Putnam, E. J. Friebele, J. Lightwave Technol. **15**, 1442 (1997).
[8] N. E. Fisher, J. Surowiec, D. J. Webb, D. A. Jackson, L. R.Gavrilov, J. W. Hand, L. Zhang, I. Bennion, Meas. Sci. Technol.**8,** 1050 (1997).
[9] N. E. Fisher, D. J. Webb, C. N. Pannell, D. A. Jackson, L. R.Gavrilov, J. W. Hand, L. Zhang, I. Bennion, Electron. Lett. **34**, 1139 (1998).
[10] N. Takahashi, A. Hirose, S. Takahashi, Opt. Rev. **4**, 691 (1997).
[11] M. G. Xu, L. Reekie, Y. T. Chow, J. P. Dakin, Electron. Lett. **29**, 398 (1993).
[12] K. P. Koo, A. D. Kersey, Optical Fiber Communication Conference, Vol. 2 of OSA Technical Digest Series -Optical Society of America, Washington, D.C.,paper ThP2, pp. 266–267, 1996.
[13] K. P. Koo, A. D. Kersey, J. Lightwave Technol. **13**, 1243 (1995).
[14] J. Hu¨ bner, P. Varming, M. Kristiansen, Electron. Lett. **33**, 139 (1997).
[15] E. Rønnekleiv, S. W. Løvseth, Thirteenth International Conference on Optical Fiber Sensors, B. Y. Kim, K. Hotate, eds., Proc. SPIE **3746**, 466 (1999).
[16] P. M. Morse, K. U. Ingard, Theoretical Acoustics – Princeton U. Press, Princeton, N.J., 1986.
[17] P. C. Riedi, An Introductionto Thermodynamics, Statistical Mechanics and KineticTheory ~MacMillan, London, 1976!, Chaps. 2; P. C. Riedi, "Second Law of Thermodynamics," in An Introduction to Thermodynamics,Statistical Mechanics and Kinetic Theory~MacMillan, London, 1976!, Chap. 3.
[18] F. P. Incropera, D. P. DeWitt, Fundamentals of Heat and Mass Transfer, 3rd ed. ~Wiley, New York, 1990.
[19] J. T. Kringlebotn, J. Archambault, L. Reekie, D. N. Payne, Opt.Lett. **19**, 2101 (1994).
[20] S. Takahashi and S. Shibita, J. Non-Cryst. Solids **30**, 359 (1978).
[21] S. W. Churchill, H. H. S. Chu, Int. J. Heat Mass Transfer **18**, 1049 (1975).
[22] S. Nakai, T. Okazaki, Int. J. Heat Mass Transfer **18**, 387 (1975).
[23] S. W. Churchill, M. Bernstein, J. Heat Transfer **99**, 300 (1977).
[24] V. T. Morgan, Advances in Heat Transfer, T. F.Irvine and J. P. Hartnett, eds. -Academic, New York, **11**, 199 (1975).
[25] J. F. Nye, Physical Properties of Crystals -Oxford U. Press, Oxford, 1985.
[26] A. Bertholds, R. Da¨ndliker, J. Lightwave Technol. **6**, 17 (1988).
[27] S. P. Timoshenko, J. N. Goodier, Theory of Elasticity~McGraw-Hill, New York, 1970.
[28] N. Lagakos, J. H. Cole, J. A. Bucaro, J. Lightwave Technol. **1**, 495 (1983).
[29] D. Marcuse, Bell Syst. Tech. J. **56**, 703 (1977).

*Corresponding author: j_j_f_l@yahoo.com